Inorg. Chem. **2007**, *46*, 1981–1991

Binuclear Iron–Sulfur Complexes with Bidentate Phosphine Ligands as Active Site Models of Fe-Hydrogenase and Their Catalytic Proton Reduction

Weiming Gao,[†] Jesper Ekström,[‡] Jianhui Liu,*[,†] Changneng Chen,[§] Lars Eriksson,[#] Linhong Weng,[¶] Björn Åkermark,*[,‡] and Licheng Sun*[,†,||]

State Key Laboratory of Fine Chemicals, DUT–KTH Joint Education and Research Center on Molecular Devices, Dalian University of Technology, 116012 Dalian, China, Department of Organic Chemistry, Arrhenius Laboratory, Stockholm University, 10691 Stockholm, Sweden, State Key Laboratory of Structural Chemistry, Fujian Institute of Research on the Structure of Matter, 350002 Fuzhou, China, Division of Structural Chemistry, Arrhenius Laboratory, Stockholm University, 10691 Stockholm, Sweden, Chemistry Department, Fudan University, 200433 Shanghai, China, and KTH Chemistry, Organic Chemistry, Royal Institute of Technology, 10044 Stockholm, Sweden

Received June 9, 2006

The displacement of CO in a few simple Fe(I)–Fe(I) hydrogenase model complexes by bisphosphine ligands $Ph_2P–(CH_2)_n–PPh_2$ [with $n = 1$ (dppm) or $n = 2$ (dppe)] is described. The reaction of $[\{\mu\text{-}(SCH_2)_2CH_2\}Fe_2(CO)_6]$ (**1**) and $[\{\mu\text{-}(SCH_2)_2N(CH_2CH_2CH_3)\}Fe_2(CO)_6]$ (**2**) with dppe gave double butterfly complexes $[\{\mu\text{-}(SCH_2)_2CH_2\}Fe_2(CO)_5(Ph_2PCH_2)]_2$ (**3**) and $[\{\mu\text{-}(SCH_2)_2N(CH_2CH_2CH_3)\}Fe_2(CO)_5(Ph_2PCH_2)]_2$ (**4**), where two Fe_2S_2 units are linked by the bisphosphine. In addition, an unexpected byproduct, $[\{\mu\text{-}(SCH_2)_2N(CH_2CH_2CH_3)\}Fe_2(CO)_5\{Ph_2PCH_2CH_2(Ph_2PS)\}]$ (**5**), was isolated when **2** was used as a substrate, where only one phosphorus atom of dppe is coordinated, while the other has been converted to P=S, presumably by nucleophilic attack on bridging sulfur. By contrast, the reaction of **1** and **2** with dppm under mild conditions gave only complexes $[\{\mu\text{-}(SCH_2)_2CH_2\}Fe_2(CO)_5(Ph_2PCH_2PPh_2)]$ (**6**) and $[\{\mu\text{-}(SCH_2)_2N(CH_2CH_2CH_3)\}Fe_2(CO)_5(Ph_2PCH_2PPh_2)]$ (**8**), where one ligand coordinated in a monodentate fashion to one Fe_2S_2 unit. Furthermore, under forcing conditions, the complexes $[\{\mu\text{-}(SCH_2)_2CH_2\}Fe_2(CO)_4\{\mu\text{-}(Ph_2P)_2CH_2\}]$ (**7**) and $[\{\mu\text{-}(SCH_2)_2N(CH_2CH_2CH_3)\}Fe_2(CO)_4\{\mu\text{-}(Ph_2P)_2CH_2\}]$ (**9**) were formed, where the phosphine acts as a bidentate ligand, binding to both the iron atoms in the same molecular unit. Electrochemical studies show that the complexes **3**, **4**, and **9** catalyze the reduction of protons to molecular hydrogen, with **4** electrolyzed already at –1.40 V versus $Ag/AgNO_3$ (–1.0 V vs NHE).

Introduction

The realization that the active site of two bacterial hydrogenases consists of a Fe_2S_2 cluster[1,2] has initiated extensive studies of such clusters.[3–5] A number of model complexes have recently been prepared, and their structures have been determined by X-ray crystallography.[6–15] The majority of these complexes have very negative redox

* To whom correspondence should be addressed. E-mail: liujh@dlut.edu.cn (J.L.), lichengs@kth.se (L.S.).
[†] Dalian University of Technology.
[‡] Department of Organic Chemistry, Stockholm University.
[§] Fujian Institute of Research on the Structure of Matter.
[#] Division of Structural Chemistry, Stockholm University.
[¶] Fudan University.
[||] Royal Institute of Technology.

(1) Peters, J. W.; Lanzilotta, W. N.; Lemon, B. J.; Seefeldt, L. C. *Science* **1998**, *282*, 1853–1858.
(2) Cammack, R. *Nature* **1999**, *397*, 214–215.
(3) Evans, D. J.; Pickett, C. J. *Chem. Soc. Rev.* **2003**, *32*, 268–275.
(4) Darensbourg, M. Y.; Lyon, E. J.; Smee, J. J. *Coord. Chem. Rev.* **2000**, *206–207*, 533–561.
(5) Frey, M. *ChemBioChem.* **2002**, *3*, 153–160.
(6) Schmidt, M.; Contakes, S. M.; Rauchfuss, T. B. *J. Am. Chem. Soc.* **1999**, *121*, 9736–9737.
(7) Lyon, E. J.; Georgakaki, I. P.; Reibenspies, J. H.; Darensbourg, M. Y. *Angew. Chem., Int. Ed.* **1999**, *38*, 3178–3180.
(8) Lawrence, J. D.; Li, H.; Rauchfuss, T. B. *Chem. Commun.* **2001**, 1482–1483.
(9) Lawrence, J. D.; Li, H.; Rauchfuss, T. B.; Bénard, M.; Rohmer, M. *Angew. Chem., Int. Ed.* **2001**, *40*, 1768–1771.
(10) Gao, W.; Liu, J.; Åkermark, B.; Sun, L. *Inorg. Chem.* **2006**, *45*, 9169–9171.
(11) Liaw, W.-F; Tsai, W.-T; Gau, H.-B; Lee, C.-M; Chou, S.-Y; Chen, W.-Y; Lee, G.-H. *Inorg. Chem.* **2003**, *42*, 2783–2788.
(12) Cloiree, A. L.; Best, S. P.; Borg, S.; Davies, S. C.; Evans, D. J.; Hughes, D. L.; Pickett, C. J. *Chem. Commun.* **1999**, 2285–2286.
(13) Lyon, E. J.; Georgakaki, I. P.; Reibenspies, J. H.; Darensbourg, M. Y. *J. Am. Chem. Soc.* **2001**, *123*, 3268–3278.
(14) Lawrence, J. D.; Rauchfuss, T. B.; Wilson, S. R. *Inorg. Chem.* **2002**, *41*, 6193–6195.
(15) Zhao, X.; Georgakaki, I. P.; Miller, M. L.; Yarbrough, J. C.; Darensbourg, M. Y. *J. Am. Chem. Soc.* **2001**, *123*, 9710–9711.

10.1021/ic0610278 CCC: $37.00
Published on Web 02/13/2007

potentials. In order to get complexes which are more readily reduced, at least after protonation, a number of phosphine complexes (PMe_3, $PPhMe_2$, $P(OMe)_3$, PPh_3)[16−19] have been prepared. Also, a bidentate ligand (dppf, 1,1′-bis(diphenylphosphino)ferrocene) has been used to give a complex where the phosphine ligand coordinates to two Fe_2S_2 units (Figure 1a).[20] With the aim of developing more efficient catalysts, we decided to study the influence of bisphosphine ligands in more depth. In principle, bidentate ligands should be capable of forming two more structural types of complexes with the Fe_2S_2 unit, one where the ligand coordinates to both iron atoms (Figure 1b) and one where it chelates to one of the same iron atoms (Figure 1c). In addition, the bidentate ligand could coordinate with only one phosphorus atom, leaving the other free for coordination to a photosensitizer, providing the possibility to create photocatalysis.[21] We have, therefore, started to investigate the coordination of bidentate phosphine ligands, which might be expected to be both more flexible and better nucleophiles than dppf. Described herein are exploratory studies of the ligands dppe and dppm, which lead to the formation of seven new complexes, [{μ-$(SCH_2)_2CH_2$}$Fe_2(CO)_5(Ph_2PCH_2)]_2$ (**3**), [{μ-$(SCH_2)_2N(CH_2CH_2CH_3)$}$Fe_2(CO)_5(Ph_2PCH_2)]_2$ (**4**), [{μ-$(SCH_2)_2N(CH_2CH_2CH_3)$}$Fe_2(CO)_5${$Ph_2PCH_2CH_2(Ph_2PS)$}] (**5**), [{μ-$(SCH_2)_2CH_2$}$Fe_2(CO)_5(Ph_2PCH_2PPh_2)$] (**6**), [{$\mu$-$(SCH_2)_2CH_2$}$Fe_2(CO)_4${$\mu$-$(Ph_2P)_2CH_2$}] (**7**), [{$\mu$-$(SCH_2)_2N(CH_2CH_2CH_3)$}$Fe_2(CO)_5$-$(Ph_2PCH_2PPh_2)$] (**8**), and [{$\mu$-$(SCH_2)_2N(CH_2CH_2CH_3)$}$Fe_2$-$(CO)_4${$\mu$-$(Ph_2P)_2CH_2$}] (**9**), which were characterized by spectroscopy and X-ray crystal structure determination.

Results and Discussion

Chemistry. Two types of Fe_2S_2 complexes were studied, a propane dithiolate (PDT) complex **1**[22] and an azapropane dithiolate (ADT) complex **2**. In order to form a vacant site and promote phosphine coordination, Me_3NO[23] and propylamine[19] were used, the amine oxide being, by far, the most efficient promoter and, therefore, being used in most cases. The known complex **1** was obtained by refluxing $Fe(CO)_5$ and 1,3-propanedithiol in toluene according to the literature method.[22] Treatment of **1** with dppe in the presence of Me_3-NO in a 1:1:1 molar ratio gave a red solid in good yield. It was characterized as [{μ-$(SCH_2)_2CH_2$}$Fe_2(CO)_5(Ph_2PCH_2)]_2$ (**3**) (Scheme 1), and we found that, like dppf,[20] the dppe ligand substitutes CO in the double monodentate manner to give a cluster of Fe_2S_2 cores antibridged by dppe. The presence of Me_3NO proved to be crucial for the success of this substitution, and no product was obtained in its absence. In the presence of excess Me_3NO and at a higher reaction temperature, the same product **3** was obtained in a pure state. The same reaction with the ADT complex **2**, prepared according to Rauchfuss's protocol,[24] gave the expected complex **4** in moderate yield. However, the reaction also gave substantial amounts of a byproduct, the complex **5** with one phosphorus atom coordinated to the Fe_2S_2 complex, while the other has been converted to a noncoordinating, terminal P═S group. Nucleophilic substitution on a coordinated thiol by phosphine or oxidative formation of elemental sulfur, which reacts with phosphine, can, perhaps, explain this remarkable transfer of sulfur from iron to phosphine.

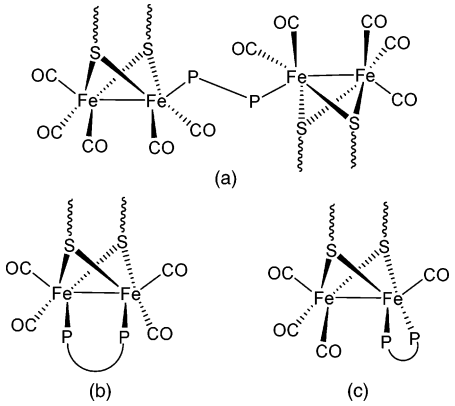

Figure 1. The possible coordination manners for a bidentate phosphine ligand.

By contrast, the reaction with the ligand dppm, where the two phosphine units are linked by only one carbon, afforded different products. The substrate and the reaction conditions are crucial for the transformation. When the reaction was carried out in acetonitrile at room temperature with **1** as a substrate, complex **6**, where the ligand is monodentate, proved to be the only product. However, when the reaction was performed in refluxing toluene, complex **7** was isolated, where the two phosphorus atoms of the dppm are connected to the two iron atoms in the same molecule (Scheme 2). Application of similar reaction conditions to **2** gave complexes **8** and **9**, which are the analogues to **6** and **7** in a variable ratio. Short reaction times, ca. 0.5 h, gave mainly **8**, while **9** was the main product when the reaction time was prolonged to 1 h. It is interesting to note that **2** is much more reactive toward the dppm than **1**. Under the same conditions (reflux, 1 h), the complex **9** was formed in 75% yield, whereas complex **1** gave only **6** in low yield. Increasing the reaction time and adding Me_3NO gave the complex **7** in ca. 30% yield.

The results of the ligand substitution in the parent clusters **1** and **2** deserve some further comments. A site-selective substitution reaction was possible by controlling reaction conditions and substrates. It is obvious that the nature of the central bridge atom (N/C), the kind of bidentate ligand (dppe/dppm), and the reaction conditions (solvent and

(16) Zhao, X.; Georgakaki, I. P.; Miller, M. L.; Mejia-Rodriguez, R.; Chiang, C.-Y.; Darensbourg, M. Y. *Inorg. Chem.* **2002**, *41*, 3917−3928.
(17) Gao, W.; Liu, J.; Åkermark, B.; Sun, L. *Inorg. Chem.* **2006**, *45*, 9169−9171.
(18) Gloaguen, F.; Lawrence, J. D.; Rauchfuss, T. B.; Benard, M.; Rohmer, M.-M. *Inorg. Chem.* **2002**, *41*, 6573−6582.
(19) Ott, S.; Borgström, M.; Kritikos, M.; Lomoth, R.; Bergquist, J.; Åkermark, B.; Hammarström, L.; Sun, L. *Inorg. Chem.* **2004**, *43*, 4683−4692.
(20) Song, L.; Yang, Z.; Bian, H.; Hu, Q. *Organometallics* **2004**, *23*, 3082−3084.
(21) Ekström, J.; Abrahamsson, M.; Olson, C.; Bergquist, J.; Kaynak, F. B.; Eriksson, L.; Sun, L.; Becker, H.-C.; Åkermark, B.; Hammarström, L.; Ott, S. *Dalton Trans.* **2006**, 4599−4606.
(22) Seyferth, D.; Womack, G. B.; Gallagher, M. K.; Cowie, M.; Hames, B. W.; Fackler, J. P.; Mazany, A. M., Jr. *Organometallics* **1987**, *6*, 283−294.
(23) Gloaguen, F.; Lawrence, J. D.; Schmidt, M.; Wilson, S. R.; Rauchfuss, T. B. *J. Am. Chem. Soc.* **2001**, *123*, 12518−12527.
(24) Li, H.; Rauchfuss, T. B. *J. Am. Chem. Soc.* **2002**, *124*, 726−727.

Scheme 1. Synthetic Route[a]

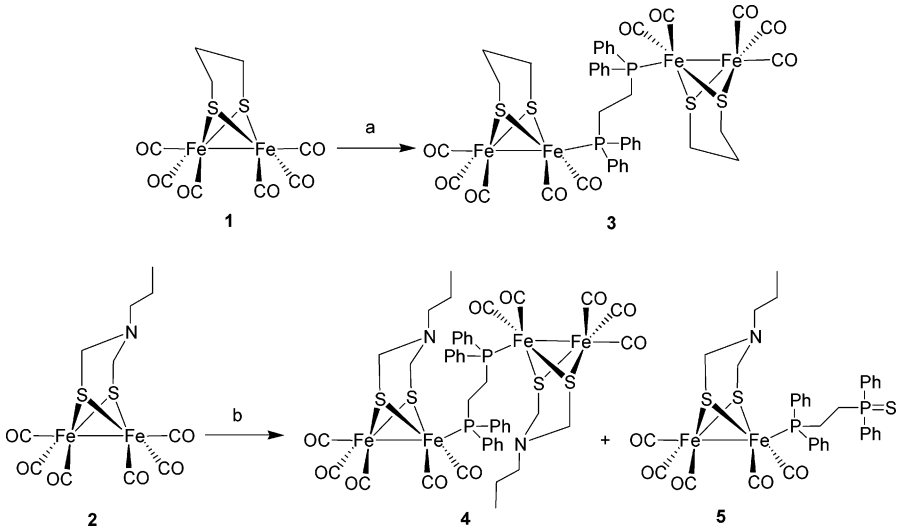

[a] Conditions: (a) CH_3CN/CH_2Cl_2, Me_3NO, dppe, rt, 1 h, 80%; (b) CH_3CN/CH_2Cl_2, Me_3NO, dppe, rt, 1 h, 60% for **4** and 23% for **5**.

Scheme 2 [a]

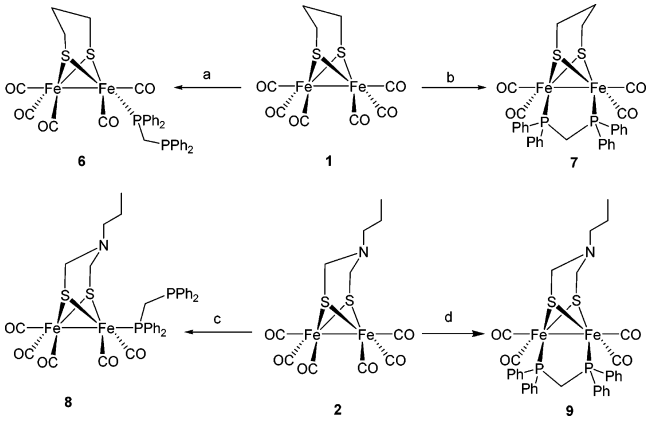

[a] Conditions: (a) CH_3CN, Me_3NO, dppm, rt, 4 h, 77%; (b) toluene, dppm, Me_3NO, reflux, 18 h, 27%; (c) toluene, dppm, reflux, 0.5 h, 50%; (d) toluene, dppm, reflux, 1 h, 75%.

temperature) significantly influence the product type of the substitution. A complex of the type a (Figure 1) was the major product when the Fe_2S_2 complexes reacted with the dppe ligand, as also reported earlier for the dppf ligand.[20] Usually, the use of CH_3CN/Me_3NO gave good yields for this transformation, but with the dppm ligand, the second phosphorus atom (e.g., **6**) did not coordinate to the second Fe_2S_2 unit, probably due to steric factors. However, in refluxing toluene, an Fe_2S_2 structure with a bridging diphosphine, such as **7**, could be obtained selectively. Similarly, the complex **9** was readily formed, preceded by the complex **8**. This suggests that complexes **6** and **8** are precursors of complexes **7** and **9**, which represent a new type of structure for complexes between bisphosphine ligands and Fe_2S_2 units.

Characterization of the Complexes. The ^{1}H NMR spectrum of complex **3** consists of the expected signals from the PDT and dppe subunits. The ^{31}P NMR spectrum shows a singlet in the typical region around 60 ppm. In the API−ES mass spectra, the most intense peak for **3** was observed at *m*/*z* 1148.7, corresponding to $[M + Cl]^-$ (negative mode), and at *m*/*z* 1114.7, corresponding to $[M + H]^+$ (positive mode). The structures of complexes **4** and **5** could also be determined by ^{1}H and ^{31}P NMR as well as by MS spectra, although both complexes exhibited broadened signals in ^{1}H NMR. The high-resolution mass spectrum of **5** gave $M^+ =$ 831.9957, which corresponds well to the formula weight with the terminal P═S double bond. The proposed structure of **5** is also clear from crystal structure data, with the expected P═S double bond being 1.95 Å, in accordance with the typical value of the P═S bond length of ca. 2.0 Å (while a P═O double bond should be ca. 1.4 Å). The ^{1}H NMR spectrum of **6** contains the expected peaks for the PDT in the region between 1.5 and 2 ppm and for the dppm at 3.3 ppm. In the ^{31}P NMR spectrum, a doublet for the coordinated P is found at 58 ppm, and a doublet for the free phosphorus is found at −25 ppm. The corresponding ^{31}P NMR spectrum for complex **7** displays one singlet at 53.65 ppm. The same trend is seen for **8** and **9**, with a pair of doublets at 57.76 and −25.2 ppm for **8** and a singlet at 54 ppm for **9**. The IR spectra of **3**, **4**, **5**, **6**, and **8** in KBr show strong absorption bands in the region of 1920−2050 cm^{-1}, corresponding to the carbonyl stretching pattern for terminally bonded C−O groups. However, for **7** and **9**, the carbonyl bands appear at lower frequencies, as might be expected for these more electron-rich complexes. For **7**, four bands are visible at 1895, 1916, 1946, and 1981 cm^{-1}, and for **9**, three bands are observed at 1916, 1952, and 1986 cm^{-1}.

The crystallographic structures of **3**−**9** are depicted in Figures 2−8, together with the atomic labeling system. Selected bond lengths and angles are given in Tables 1−7. The main framework of clusters **3** and **4** (Fe−P−C−C−P−Fe) is composed of zigzag structures with one Fe_2S_2 butterfly unit attached to each end of the dppe bridge. Each Fe_2S_2 subunit has a square pyramidal structure, and both complexes have C_{2v} symmetry. The Fe_2S_2 cores in the tetranuclear complex **3** and the parent complex **1** are geometrically similar. The Fe−Fe bond distance is equal to that in **1** (2.51 Å), showing that the ligand exchange has no effect on the Fe−Fe bond length. The P(1)−Fe(1)−Fe(2) plane is almost parallel to that of P(1A)−Fe(1A)−Fe(2A) because of an

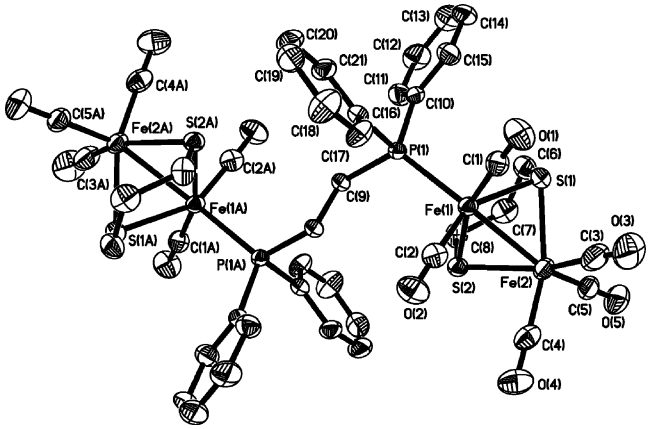

Figure 2. ORTEP (ellipsoids at 30% probability) diagram of **3**.

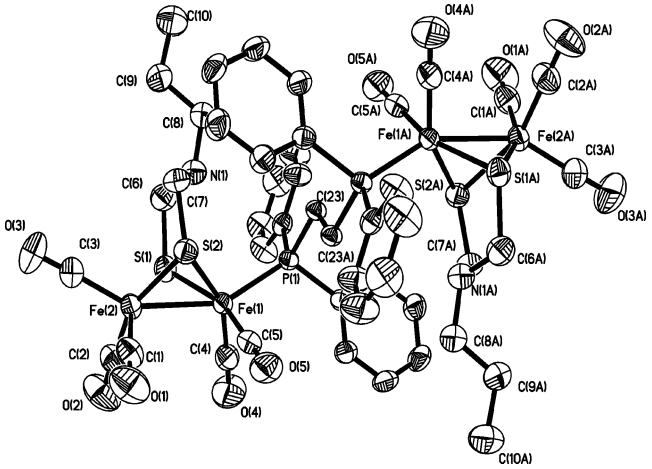

Figure 3. ORTEP (ellipsoids at 30% probability) diagram of **4**.

Table 1. Selected Bond Lengths and Angles for Complex **3**

bond lengths (Å)		bond angles (°)	
Fe(1)−Fe(2)	2.5108(14)	Fe(1)−S(1)−Fe(2)	67.42(6)
Fe(1)−S(1)	2.262(2)	Fe(1)−S(2)−Fe(2)	67.30(6)
Fe(1)−S(2)	2.2587(19)	S(1)−Fe(1)−S(2)	84.54(7)
Fe(2)−S(1)	2.262(2)	S(1)−Fe(2)−S(2)	84.22(7)
Fe(2)−S(2)	2.273(2)	P(1)−Fe(1)−Fe(2)	151.23(6)
Fe(1)−C(1)	1.774(8)	C(10)−P(1)−Fe(1)	114.5(2)
Fe(1)−C(2)	1.764(8)	C(10)−P(1)−C(16)	102.3(3)
Fe(1)−P(1)	2.2212(19)	C(9)−P(1)−C(16)	99.7(3)
P(1)−C(10)	1.826(6)	C(9A)−C(9)−P(1)	112.3(5)
P(1)−C(16)	1.841(7)		
S(1)−C(6)	1.821(7)		
S(2)−C(8)	1.143(8)		

Table 2. Selected Bond Lengths and Angles for Complex **4**

bond lengths (Å)		bond angles (°)	
Fe(1)−Fe(2)	2.5101(8)	Fe(1)−S(1)−Fe(2)	67.38(4)
Fe(1)−S(1)	2.2626(13)	Fe(1)−S(2)−Fe(2)	67.27(4)
Fe(1)−S(2)	2.2632(12)	S(1)−Fe(1)−S(2)	84.27(5)
Fe(2)−S(1)	2.2625(13)	S(1)−Fe(2)−S(2)	84.15(5)
Fe(2)−S(2)	2.2686(13)	P(1)−Fe(1)−Fe(2)	151.42(4)
Fe(1)−C(4)	1.783(5)	C(23A)−C(23)−P(1)	111.5(3)
Fe(1)−C(5)	1.780(5)	C(11)−P(1)−C(17)	100.14(19)
Fe(1)−P(1)	2.2330(11)		

inversion center at the midpoint of the CH_2CH_2 bond. The substitution of CO is site selective, and the phosphine in **3** occupies only the two apical positions, which is consistent with the behavior of the usual monophosphine ligands.[16−19] Viewed along the C(9)−C(9A) bond, P(1) and P(1A) are in

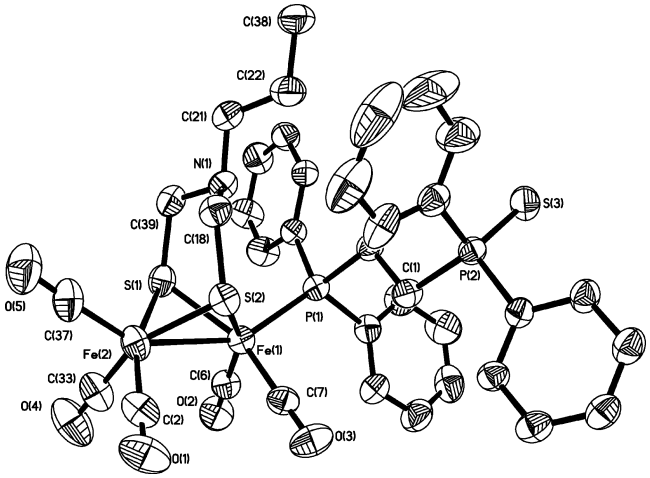

Figure 4. ORTEP (ellipsoids at 30% probability) diagram of **5**.

Table 3. Selected Bond Lengths and Angles for Complex **5**

bond lengths (Å)		bond angles (°)	
Fe(1)−Fe(2)	2.5165(12)	Fe(1)−S(1)−Fe(2)	67.94(5)
Fe(1)−S(1)	2.2557(15)	Fe(1)−S(2)−Fe(2)	67.57(4)
Fe(1)−S(2)	2.2566(14)	S(1)−Fe(1)−S(2)	84.27(5)
Fe(2)−S(1)	2.2481(16)	S(1)−Fe(2)−S(2)	84.16(5)
Fe(2)−S(2)	2.2688(17)	C(18)−N(1)−C(39)	113.9(4)
Fe(1)−C(6)	1.756(5)	C(1)−P(2)−S(3)	113.39(18)
Fe(1)−C(7)	1.756(6)		
Fe(1)−P(1)	2.2169(13)		
P(2)−C(1)	1.819(4)		
P(2)−S(3)	1.9445(18)		

a staggered (antiperiplanar), rather than eclipsed, conformation. The C(10)−P(1)−C(16) angle is 102.3°, significantly smaller than the typical value (ca. 109°), which is an indication of the steric bulk of the two Fe_2S_2 subunits. The structure of **4** is very similar to that of **3**. The C(11)−P(1)−C(17) (not all labeled for clarity) angle value is 100.1°, even

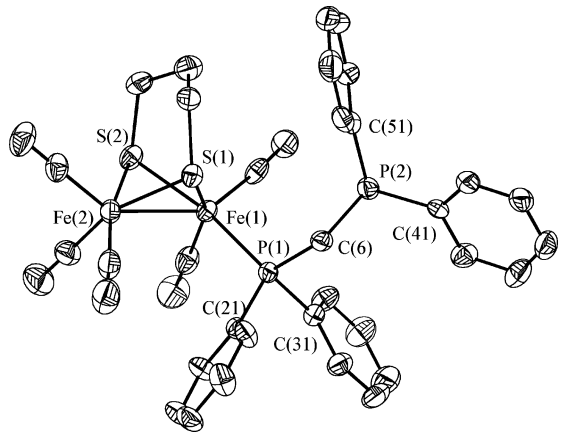

Figure 5. ORTEP (ellipsoids at 30% probability) diagram of **6**.

Table 4. Selected Bond Lengths and Angles for Complex **6**

bond lengths (Å)		bond angles (°)	
Fe(1)−Fe(2)	2.5651(8)	Fe(1)−S(1)−Fe(2)	69.14(3)
Fe(2)−S(1)	2.2582(12)	Fe(1)−S(2)−Fe(2)	69.25(3)
Fe(2)−S(2)	2.2591(13)	S(1)−Fe(1)−S(2)	85.05(4)
Fe(1)−S(1)	2.2607(11)	S(1)−Fe(2)−S(2)	85.05(4)
Fe(1)−S(2)	2.2555(10)	P(1)−C(6)−P(2)	113.12(18)
Fe(1)−P(1)	2.2400(10)	C(21)−P(1)−C(31)	100.58(19)
		C(6)−P(2)−C(41)	100.08(16)
		C(6)−P(2)−C(51)	102.14(19)
		C(41)−P(2)−C(51)	103.23(19)

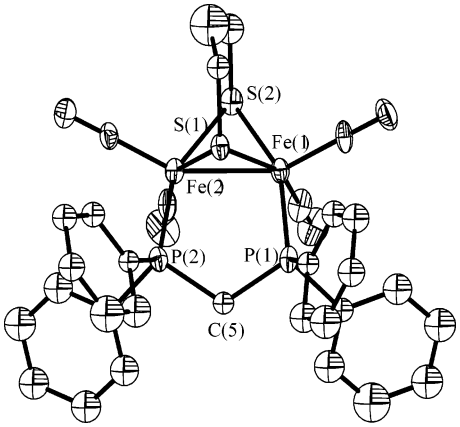

Figure 6. ORTEP (ellipsoids at 30% probability) diagram of **7**.

Table 5. Selected Bond Lengths and Angles for Complex **7**

bond lengths (Å)		bond angles (°)	
Fe(1)−Fe(2)	2.5154(18)	Fe(1)−S(1)−Fe(2)	67.78(8)
Fe(1)−S(1)	2.255(3)	Fe(1)−S(2)−Fe(2)	67.85(9)
Fe(1)−S(2)	2.252(3)	S(1)−Fe(1)−S(2)	84.53(11)
Fe(2)−S(1)	2.256(3)	S(1)−Fe(2)−S(2)	84.44(11)
Fe(2)−S(2)	2.255(3)	P(1)−C(5)−P(2)	115.8(5)
Fe(1)−P(1)	2.220(3)		
Fe(2)−P(2)	2.219(3)		

smaller than the corresponding angle C(10)−P(1)−C(16) in **3**, probably due to the interaction with the nearby *n*-propyl. For complexes **4** and **5**, the bond lengths and angles at the central dinuclear units are very close to those reported earlier for complexes related to **1**.[19] In complex **5**, the monodentate phosphine ligand also coordinates to an apical position, as visualized in Figure 4. A comparison of complexes **3**, **4**, and **5** shows that the Fe(1)−P(1) bond distances are almost the same, all falling in the range of 2.22−2.23 Å. The angle of C(9A)−C(9)−P(1) in **3** is 112.3°, a little larger than the

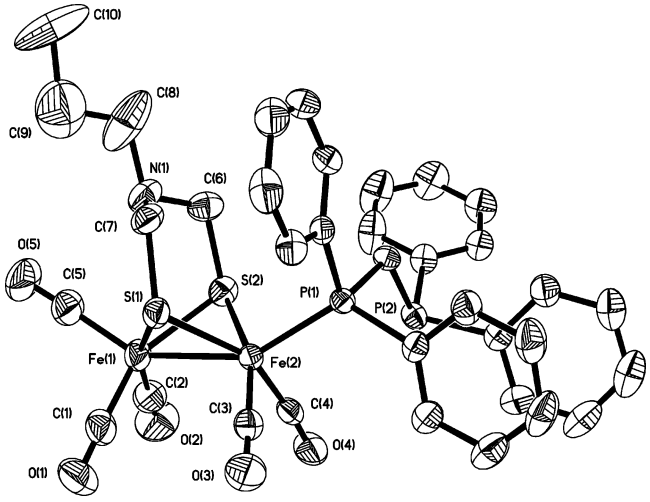

Figure 7. ORTEP (ellipsoids at 30% probability) diagram of **8**.

Table 6. Selected Bond Lengths and Angles for Complex **8**

bond lengths (Å)		bond angles (°)	
Fe(1)−Fe(2)	2.5217(6)	Fe(1)−S(1)−Fe(2)	68.15(3)
Fe(2)−S(1)	2.2434(9)	Fe(1)-S(2)−Fe(2)	67.86(3)
Fe(2)−S(2)	2.2539(10)	S(1)−Fe(1)−S(2)	83.96(3)
Fe(1)−S(1)	2.2577(10)	S(1)−Fe(2)−S(2)	84.52(4)
Fe(1)−S(2)	2.2639(11)	P(1)−C(35)−P(2)	112.32(16)
Fe(2)−P(1)	2.2168(9)		

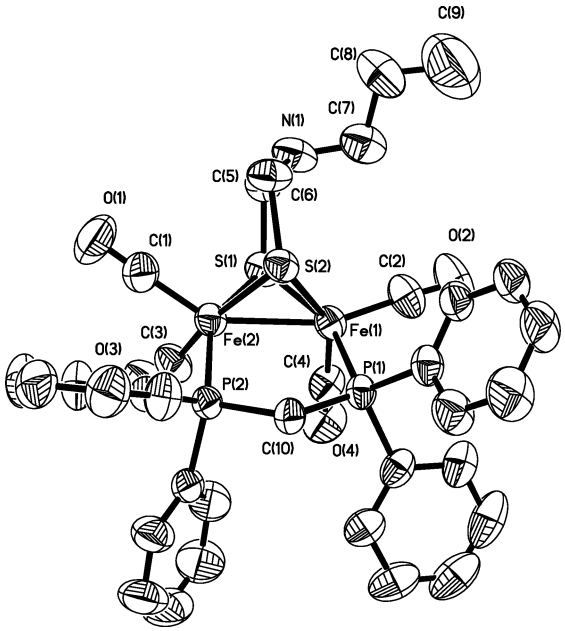

Figure 8. ORTEP (ellipsoids at 30% probability) diagram of **9**.

Table 7. Selected Bond Lengths and Angles for Complex **9**

bond lengths (Å)		bond angles (°)	
Fe(1)−Fe(2)	2.5044(6)	Fe(1)−S(1)−Fe(2)	67.69(3)
Fe(2)−S(1)	2.2579(9)	Fe(1)−S(2)−Fe(2)	66.66(3)
Fe(2)−S(2)	2.2652(8)	S(1)−Fe(1)−S(2)	84.15(3)
Fe(1)−S(1)	2.2384(9)	S(1)−Fe(2)−S(2)	84.34(3)
Fe(1)−S(2)	2.2923(9)	P(1)−C(10)−P(2)	113.68(15)
Fe(1)−P(1)	2.2005(9)		
Fe(2)−P(2)	2.2393(9)		

corresponding angle in **4**, which is 111.5°. The P−CH_2−CH_2−P chain is thus a little more compressed in **4**. Notably, the propyl groups on the bridgehead N of both **4** and **5** point toward the bulky dppe moiety, which occupies a thermodynamically unstable position.

Passing from dppe to dppm, there are clear structural changes, as shown by the structure **6**. The Fe−Fe bond distance increases from 2.51 Å in complex **3** to 2.56 Å in complex **6**. This somewhat exceeds the bond length in the complex with a ferrocenyl−bisphosphine ligand (2.543 Å).[20] The second phosphorus atom is neither coordinated to Fe nor combined with the sulfur atom, in contrast to the dppe ligand. In complexes **3**, **4**, and **5**, the phosphine occupies an apical position, whereas in complex **6**, it occupies a basal position, perhaps for steric reasons. The Fe(1)−P(1) bond distance in **6** is ca. 2.24 Å, slightly longer than that in **3** and **4**. In contrast to the basal coordination in **6**, the phosphine is in an axial position in **8**. Both the Fe−Fe bond (2.52 Å) and the Fe−P bond (∼2.22 Å) in **8** are shorter than the corresponding bond in **6**, and they are of approximately the same length as the bonds in **3**, **4**, and **5**.

For complexes **7** and **9**, the dppm bridges the two iron atoms with one phosphorus atom bonded to each iron atom. The phosphorus atoms both occupy basal positions. The Fe(1)−P(1) distance (2.20 Å) is a little shorter than the Fe(2)−P(2) distance (2.24 Å) in **9**, but in **7**, they are essentially equal. The P−C−P bond angles in complexes **6**, **8**, and **9**

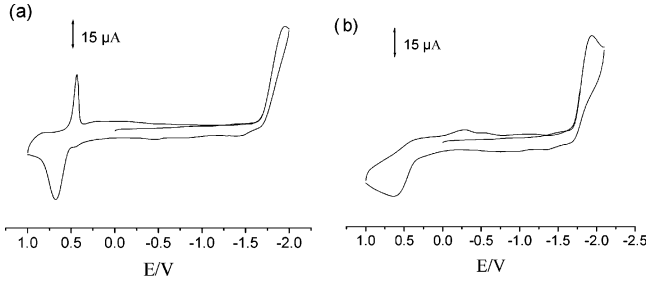

Figure 9. Cyclic voltammograms of **3** (a) and **4** (b) (1.0 mM) in 0.05 M *n*-Bu_4NPF_6/CH_2Cl_2 at a scan rate of 100 mV/s.

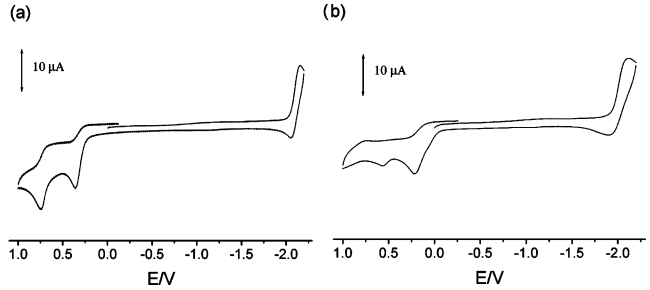

Figure 10. Cyclic voltammogram of **7** (a) and **9** (b) (1.0 mM) in 0.05 M *n*-Bu_4NPF_6/CH_3CN at a scan rate of 100 mV/s.

are about 113°, although their coordination manners are different. In **7**, this angle is slightly bigger, 115.8°.

Electrochemistry. In order to get an estimate of the capability to catalyze hydrogen production, cyclic voltammetry (CV) of the complexes **3**, **4**, **7**, and **9** (Figures 9 and 10) was performed. Complex **3** exhibited an irreversible oxidation wave at 0.67 V ($Fe^IFe^I/Fe^{II}Fe^I$) and an irreversible reduction peak at −1.94 V (Fe^IFe^I/Fe^0Fe^I) (vs $Ag/AgNO_3$). Complex **4** showed a broad irreversible oxidation peak at 0.62 V and an irreversible reduction peak at −1.93 V. This is in agreement with the published CVs of other types of related complexes.[18,25−29] Complex **7** showed two irreversible oxidation waves at 0.36 ($Fe^IFe^I/Fe^{II}Fe^I$) and 0.74 V($Fe^IFe^{II}/Fe^{II}Fe^{II}$),[30,37]as well as an irreversible reduction peak at −2.14 V (Fe^IFe^I/Fe^0Fe^I) (vs $Ag/AgNO_3$). Similarly, complex **9** showed two irreversible oxidation peaks at 0.22 and 0.56 V and an irreversible reduction peak at −2.11 V. Controlled potential coulometry of complexes **3** and **4** at −2 V in the absence of acid showed a consumption of 2.10 and 2.13 electrons per molecule. This suggests that the two Fe_2S_2 centers are essentially identical and mutually independent and are both reduced one step at ca. −2 V.

The influence of strong acid CF_3SO_3H (0−40 equiv) on complexes **3**, **4**, **7**, and **9** was studied by CV (Figures 11 and 12). At moderate acid concentration (0 to 20 equiv), the oxidation peak at 0.62 V for complex **4** moved to a more positive potential by 0.24 V. A new reduction peak appeared at about −1.25 V when 2 equiv of CF_3SO_3H was added. This shift upon protonation (ca 0.6 V) is greater than the corresponding shift (0.23 V) for a related hexacarbonyl complex,[30] perhaps because of the replacement of a carbonyl group by a phosphine ligand. As the acid concentration was increased, the peaks at −1.25 and −2 V both grew and moved to more negative potentials (Figure 11b). These features are indicative of catalytic proton reduction. By contrast, no new reduction peaks were detected for complex **3**, and the original one did not move to a more negative potential when CF_3SO_3H was added, although it also grew larger (Figure 11a). At high acid concentration, curve crossing was observed for both complexes **3** and **4** (vide infra).[31,36]

The CVs of complexes **7** and **9** in the presence of triflic acid in CH_3CN gave similar results as **3** and **4**. For **7**, except that the current intensities of all reduction peaks grew further with the increase of the acid concentration, no other new changes were observed. By contrast, for **9**, a new reduction peak appeared at about −1.6 V when 1 equiv of CF_3SO_3H was added. This shift value upon protonation (ca. 0.5 V) is comparable to that for **4** (0.6 V). However, with complexes **7** and **9**, curve crossing could not be observed even at a high acid concentration. The oxidation peaks of **9** were clearly shifted to more positive potentials when acid was added in a slightly more complicated manner (Figure 12). The second oxidation peak at 0.56 V ($Fe^IFe^{II}/Fe^{II}Fe^{II}$) moved to more positive potential (0.83 V).[37] After addition of 2 equiv of acid, the first oxidation at 0.22 V ($Fe^IFe^I/Fe^{II}Fe^I$) disappeared completely, and only one oxidation peak at ca. 0.83 V was observed. This was true also after addition of 40 equiv of acid. A possible explanation is that the two iron atoms become essentially equivalent when the nitrogen is protonated.

The mechanisms for H_2 formation are not clear. An ECCE (electrochemical−chemical−chemical−electrochemical) mechanism, which has been suggested for a related complex,[31] can tentatively be assigned for complex **3**, although an ECEC (electrochemical−chemical−electrochemical−chemical) mechanism is also possible (vide infra). For **4**, a somewhat different mechanism seems probable since the first step is protonation of the two bridgehead nitrogens, leading to a well-defined complex $\mathbf{4H_2}^{2+}$. This results in a new reduction peak at −1.25 V, and the carbonyl frequencies in the IR spectrum are shifted by 10−18 cm^{-1} to a higher frequency relative to those of the parent **4**. This is of the same magnitude as those observed for a related bis(trimethylphosphine) complex.[35] The methylene protons of $\mathbf{4H_2}^{2+}$, in

(25) Gloaguen, F.; Lawrence, J. D.; Rauchfuss, T. B. *J. Am. Chem. Soc.* **2001**, *123*, 9476−9477.
(26) Chong, D.; Georgakaki, I. P.; Mejia-Rodriguez, R.; Sanabria-Chinchilla, J.; Soriaga, M. P.; Darensbourg, M. Y. *J. Chem. Soc., Dalton Trans.* **2003**, 4158−4163.
(27) Liaw, W.-F.; Lee, N.-H.; Chen, C.; Lee, C.-M.; Lee, G.-H.; Peng, S.-M. *J. Am. Chem. Soc.* **2000**, *122*, 488−494.
(28) Razavet, M.; Davies, S. C.; Hughes, D. L.; Barclay, J. E.; Evans, D. J.; Fairhurst, S. A.; Liu, X.; Pickett, C. J. *J. Chem. Soc., Dalton Trans.* **2003**, 586−595.
(29) Liu, T.; Wang, M.; Shi, Z.; Cui, H.; Dong, W.; Chen, J.; Åkermark, B.; Sun, L. *Chem.—Eur. J.* **2004**, *10*, 4474−4479.
(30) Ott, S.; Kritikos, M.; Åkermark, B.; Sun, L.; Lomoth, R. *Angew. Chem., Int. Ed.* **2004**, *43*, 1006−1009.
(31) Mejia-Rodriguez, R.; Chong, D.; Reibenspies, J. H.; Soriaga, M. P.; Darensbourg, M. Y. *J. Am. Chem. Soc.* **2004**, *126*, 12004−12014.
(32) Houmam, A.; Hamed, E. M.; Still, I. W. J. *J. Am. Chem. Soc.* **2003**, *125*, 7258−7265.
(33) Kuchynka, D. J.; Kochi, J. K. *Inorg. Chem.* **1988**, *27*, 2574−2581.
(34) Saveant, J. M. *Acc. Chem. Res.* **1980**, *13*, 323−329.
(35) Schwartz, L.; Eilers, G.; Eriksson, L.; Gogoll, A.; Lomoth, R.; Ott, S. *Chem. Commun.* **2006**, 520−522.
(36) Bard, A. J.; Faulkner, L. R. *Electrochemical Methods*, 2nd ed.; Wiley: New York, 2001.
(37) Li, P.; Wang, M;. He, C.; Li, G.; Liu, X;. Chen, C.; Åkermark, B.; Sun, L. *Eur. J. Inorg. Chem.* **2005**, 2506−2513.

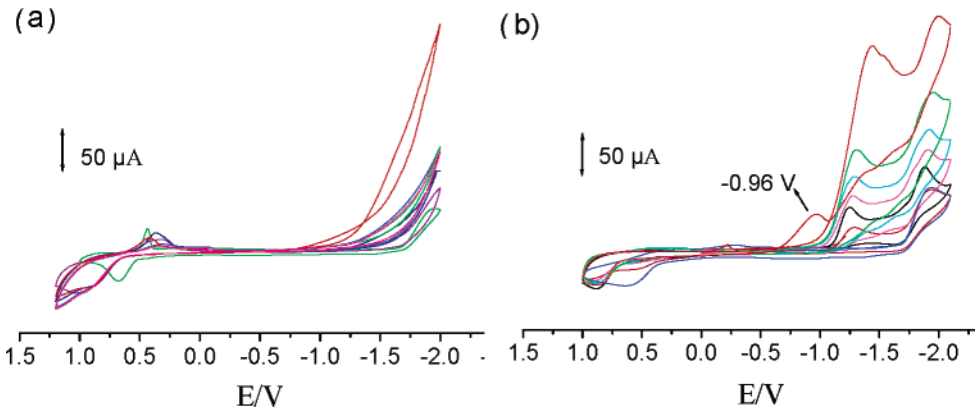

Figure 11. Cyclic voltammogram of **3** (a) and **4** (b) (1.0 mM) with addition of CF_3SO_3H (0, 2, 6, 10, 16, 20, 40 equiv) in 0.05 M *n*-Bu_4NPF_6/CH_2Cl_2 at a scan rate of 100 mV/s. The curves for acid concentrations between 20−40 equiv were omitted for clarity (see Figure S2).

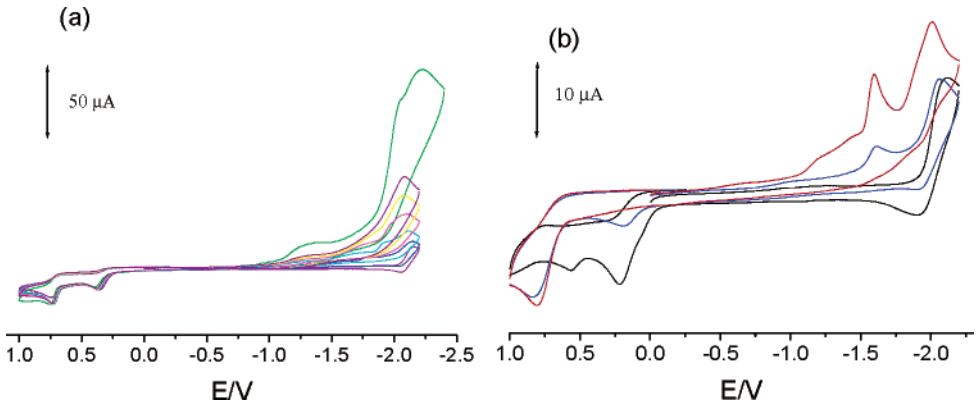

Figure 12. Cyclic voltammogram of **7** (a) (1.0 mM) with addition of CF_3SO_3H (0, 1, 2, 3, 4, 5, 10 equiv) and **9** (b) (1.0 mM) with addition of CF_3SO_3H (0, 1, 2 equiv) in 0.05 M *n*-Bu_4NPF_6/CH_3CN at a scan rate of 100 mV/s. The curves for acid concentrations between 5 and 10 equiv for **9** were omitted for clarity (see Figure S3).

proximity to the ADT nitrogen (−NCH_2S−), moved from 2.66 (singlet) and 2.12 ppm (singlet) in **4** to 4.30 (multiplet) and 3.05 ppm (doublet) (ratio of 1:1). The peak in the ^{31}P NMR, finally, moved from 60.45 to 62.50 ppm (see Experimental Section). The protonation could be completely reversed by the addition of 5 equiv of aniline to regenerate **4**. However, when the same amount of 4-cyanoaniline was added, no change occurred, placing the pK_a of $\mathbf{4H_2}^{2+}$ between 10.6 and 7.6. If we represent half of $\mathbf{4H_2}^{2+}$ by $(Fe^IFe^INH)^+$, (Fe^0Fe^INH) should be formed by the reduction at ca. −1.25 V. Protonation will then give $(HFe^{II}Fe^INH)^+$, which could react with a second proton to give molecular hydrogen and $(Fe^{II}Fe^INH)^{2+}$. After a second reduction, $(Fe^IFe^INH)^+$, corresponding to $\mathbf{4H_2}^{2+}$, would be regenerated, in accordance with the mechanism suggested above for **3** and earlier for related complexes.[31] However, since the hydride in $(HFe^{II}Fe^INH)^+$ might be expected to have more proton than hydride character, the reaction sequence may, in fact, be reduction to (HFe^IFe^INH) first, generating a complex with stronger hydride character, followed by protonation to give hydrogen and $\mathbf{4H_2}^{2+}$ directly. The mechanism could then tentatively be presented as a CECEC (chemical−electrochemical−chemical−electrochemical−chemical) mechanism (Scheme 3). Upon short bulk electrolysis (5−10 min) of **4** in a strongly acidic acetonitrile solution, two sets of carbonyl frequencies can be observed by IR spectroscopy, one at 2062 and 2003 cm^{-1} and the other

Scheme 3. Possible Mechanism of the Proton Reduction

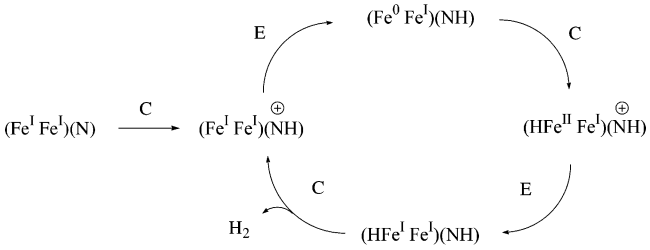

at 2155 and 2121 cm^{-1}. The first most probably corresponds to $\mathbf{4H_2}^{2+}$. The second species could be $(HFe^{II}Fe^INH)^+$ since the shifts in the carbonyl frequencies, 93 and 118 cm^{-1}, are of the same magnitude as those observed upon protonation of related Fe^IFe^I−bis(trimethylphosphine) complexes,[31,35] which are around 80 cm^{-1}.

The interpretation of the curve crossing that was observed in the CVs of complexes **3** and **4** is not clear. This type of behavior was recently also observed for the related complex [(μ-PDT)$Fe_2(CO)_4L_2$] (L = PTA).[31] The crossing was barely visible for **3**, even upon addition of 40 equiv of acid (Figure 11a), while a distinct new peak could be observed at −0.96 V upon the return scan for **4** (Figure 11b). The reduction peak currents (ip) at ca. −1.94 V for **3** and −1.25 V for **4** were plotted versus scan rates from 60 to 800 mV/s in the absence of acid and at an acid concentration of 40 equiv. For **4**, a square-root relationship between ip and the scan rate was obtained, which is an indication that the "curve-

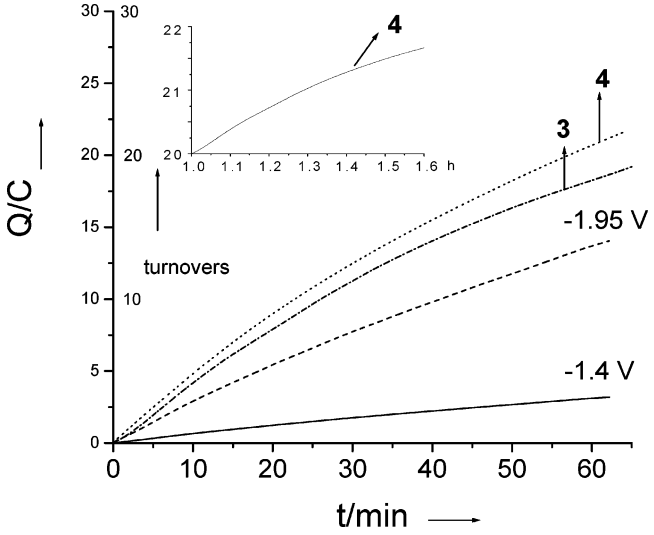

Figure 13. Coulometry for bulk electrolysis: CF_3SO_3H (100 mM) in the presence of **3** (— · —), **4** (· · ·), and the baselines electrolyzing at −1.40 V (——) and −1.95 V (- - -). Electrolysis potentials: −1.95 V for **3** and −1.4 V for **4** (vs $Ag/AgNO_3$). Solution volume: 5 mL. Glassy carbon electrode surface area: 1.1 cm^2; all measurements were made on 1 mM solutions of the relevant complexes in CH_2Cl_2 with *n*-Bu_4NPF_6 (0.1 M) as the supporting electrolyte.

crossing" peak is not the result of a surface deposition process.[31] For **3**, this relationship was not obtained, indicating that the surface deposition may occur. For **4**, not only does surface crossing take place, but the formation of a new intermediate is suggested by the observation of a distinct peak at −0.96 V subsequent to the reduction of **4** at ca. −2 V.[32−34] As far as we are aware, this type of behavior has not been observed before. Further work is, therefore, necessary in order to establish the nature of this intermediate.

Finally, catalytic generation of hydrogen was studied by controlled potential electrolysis of complexes **3**, **4**, and **9** in CH_2Cl_2− or CH_3CN−Bu_4NPF_6 (Figure 13 and 14). During the recording of the CVs of complexes **3**, **4**, **7**, and **9**, we could observe hydrogen bubbles evolving from the surface of the glassy carbon disc electrode for three complexes when enough CF_3SO_3H was added. The electrochemistry of the complexes was, therefore, studied in more detail. As might be expected, some uncatalyzed proton reduction could be observed upon addition of the strong triflic acid, even in the absence of catalyst. At the potential required for the reduction of **3** (1.95 V vs $Ag/AgNO_3$), the rate of uncatalyzed hydrogen evolution was fairly high, but a small catalytic activity of **3** could be observed (Figure 13). At −1.4 V, which was sufficient for reduction in the presence of complex **4**, the rate of uncatalyzed reduction was considerably smaller, and a distinct catalytic activity of **4** could be observed. However, in both cases, the catalytic activity decreased with time and ceased, at last, for **3**, after 50 min and for **4**, after 1.5 h. On the basis of each Fe_2S_2 unit, this corresponds to ca. 4 turnovers for **3** and 12 for **4**. Since **7** required a reduction potential of −2.1 V, we did not study its hydrogen evolution. Complex **9** showed hydrogen evolution with a turnover number of ca. 14 at −1.85 V (Figure 14). The less negative electrolysis potentials and relatively higher efficiency for **4** and **9** show that they are better catalysts for reduction of protons.

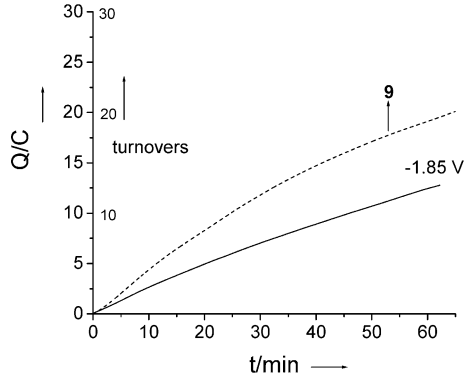

Figure 14. Coulometry for bulk electrolysis: CF_3SO_3H (100 mM) in the presence of **9** (- - -) and the baselines electrolyzing at −1.85 V (——). Electrolysis potentials: −1.85 V for **9** (vs $Ag/AgNO_3$). Solution volume: 5 mL. Glassy carbon electrode surface area: 1.1 cm^2; all measurements were made on 1 mM solutions of the relevant complexes in CH_3CN with *n*-Bu_4NPF_6 (0.1 M) as the supporting electrolyte.

Conclusion

The reaction of the Fe_2S_2 complexes **1** and **2** with the bisphosphines dppe and dppm has been found to give three types of complexes, depending on reaction conditions and the structure of the phosphine. With dppe, under fairly mild reaction conditions, both **1** and **2** gave structures that contain two terminal butterfly Fe_2S_2 cluster cores coordinated to a bisphosphine ligand (**3**, **4**). In the case of **2**, also ca. 20% of complex **5** was formed, where one phosphine had been converted to a phosphine sulfide. Under more forcing conditions, this became the major product. By contrast, using the ligand dppm, the bisphosphine was only monodentate, giving complex **6**, probably because the combined bulk of two phenyl groups and the coordinated complex decreased the reactivity of the second phosphorus for steric reasons. However, under forcing conditions, the reactions with dppm gave complexes **7** and **9**, in which the diphosphine ligand bridges the two Fe atoms of the same molecule. This shows that, depending on complex, phosphine, and reaction conditions, a great variety of complexes can be prepared selectively. Finally, it was found that complex **4** is a good catalyst for electrochemical production of hydrogen with a relatively low reduction potential in the presence of an acid.

Experimental Section

All reactions and operations related to organometallic complexes were carried out under a dry, oxygen-free, nitrogen atmosphere with standard Schlenk techniques. All solvents were dried and distilled prior to use according to the standard methods. Commercially available chemicals, including *n*-propylamine, paraformaldehyde, dppe, and dppm were used without further purification. The reagents $LiEt_3BH$ and triflic acid were purchased from Aldrich.

Infrared spectra were recorded on a JASCO FT/IR 430 spectrophotometer. ^1H and ^{13}C NMR (mainly $CDCl_3$ solution) were collected on a Varian INOVA 400 NMR spectrometer. Mass spectra were recorded on an HP1100 MSD instrument, and HRMS was performed on a HPLC-Q-TOFMS (Micro) system. Gas chromatograms were recorded on a GC7890, and nitrogen was selected as the carrier gas.

Methylene chloride (Aldrich, spectroscopy grade), used for performance of electrochemistry, was dried with molecular sieves

(4 Å) and then freshly distilled from CaH_2 under N_2. A solution of 0.05 M *n*-Bu_4NPF_6 (Fluka, electrochemical grade) in CH_2Cl_2 or CH_3CN was used as the electrolyte. Electrochemical measurements were recorded using a BAS-100W electrochemical potentiostat. The electrolyte solution was degassed by bubbling with dry argon for 10 min before measurement. Cyclic voltammograms were obtained in a three-electrode cell under argon. The working electrode was a glassy carbon disc (diameter 3 mm), successively polished with 3 and 1 μm diamond pastes and sonicated in ion-free water for 10 min. The reference electrode was a nonaqueous Ag/Ag^+ electrode (1.0 mM $AgNO_3$ in CH_3CN), and the auxiliary electrode was a platinum wire. The gas in the airtight vessel was carefully taken out by syringe, which was hydrogen identified by gas chromatography. Gas chromatography was performed under isothermal conditions with nitrogen as a carrier gas and a thermal conductivity detector (TCD).

Single-crystal X-ray diffraction patterns were recorded with an Oxford Diffraction Excalibur diffractometer equipped with a sapphire-3 CCD on a Mo radiation source ($\lambda = 0.71073$ Å) with ω scans at different ϕ's to fill an Ewald sphere. The sample−detector distance was 50 mm. The maximum 2θ was ≈63°.

Indexing, cell refinements, and integration of reflection intensities were performed with the Crysalis software.[38] Numerical absorption correction was performed with the program X-RED,[39] verifying the crystal shape with the program X-shape.[40] The structure was solved by direct methods using SHELXS97,[41] giving electron density maps where most of the non-hydrogen atoms could be resolved. The rest of the non-hydrogen atoms were located from difference electron density maps, and the structure model was refined with full-matrix least-squares calculations on F^2 using the program SHELXL97-2.[42] All non-hydrogen atoms were refined with anisotropic displacement parameters, and the hydrogens, which were placed at geometrically calculated positions and let to ride on the atoms they were bonded to, were given isotropic displacement parameters calculated as $\xi \cdot U_{eq}$ for the non-hydrogen atoms with $\xi = 1.2$ for methylenic ($-CH_2-$) and aromatic hydrogens.

Synthesis of [{μ-$(SCH_2)_2N(CH_2CH_2CH_3)$}$Fe_2(CO)_6$] (2). A solution of *n*-propylamine (3.3 mL, 40 mmol) and paraformaldehyde (2.4 g, 80 mmol) in THF (40 mL) was stirred for 4 h, cooled to 0 °C, and $(HS)_2Fe_2(CO)_6$ (2 mmol) in THF (40 mL) was added. After further reaction for 5 h, the solution was filtered, and the solvent was removed on a rotary evaporator. The crude product was purified by chromatography on silica gel with hexane as the eluent to give **2** (770 mg, 90%) as a red solid. ^{1}H NMR ($CDCl_3$): δ 0.79 (s, 3H, CH_3), 1.31 (s, 2H, $CH_3CH_2CH_2$), 2.61 (s, 2H, CH_2CH_2N), 3.51 (s, 4H, 2 × NCH_2S) ppm. IR (KBr): ν(CO) 2073, 2030, and 1992 cm^{-1}. MS (API−ES): *m*/*z* 430.0 $[M + H]^+$. Anal. Calcd (%) for $C_{11}H_{11}Fe_2NO_6S_2$: C, 30.79; H, 2.58; N, 3.26. Found: C, 30.37; H, 2.82; N, 3.27.

Synthesis of [{μ-$(SCH_2)_2CH_2$}$Fe_2(CO)_5(Ph_2PCH_2)$]$_2$ (3). A solution of **1** (0.193 g, 0.5 mmol) and $Me_3NO\cdot 2H_2O$ (0.111 g, 1 mmol) dissolved in MeCN (40 mL) was stirred for 5 to 10 min at room temperature. Then, a solution of dppe (0.199 g, 0.5 mmol), dissolved in CH_2Cl_2 (2 mL), was added. After 1 h, the solvent was evaporated, and the crude product was purified by chromatography on silica gel with CH_2Cl_2/hexane (1/2 v/v) as the eluent to give **3** (220 mg, 80%). ^{1}H NMR ($CDCl_3$): δ 0.87−0.90 (m, 4H, 2 × $CH_2CH_2CH_2$), 1.49−1.50 (m, 4H, 2 × SCH_2CH_2), 1.76−1.79 (m, 4H, 2 × SCH_2CH_2), 2.58 (s, 4H, PCH_2CH_2P), 7.40−7.33 (m, 12H, Ph), 7.51−7.49 (m, 8H, Ph) ppm. ^{31}P NMR ($CDCl_3$): δ 60.66 (s) ppm. IR (KBr): ν(CO) 2040, 1982, and 1922 cm^{-1}. MS (API−ES): *m*/*z* 1114.7 $[M + H]^+$, 1148.7 $[M + Cl]^-$. HRMS (ESI): *m*/*z* $[M + Cl]^-$ calcd for $C_{42}H_{36}Fe_4O_{10}P_2S_4Cl$, 1148.7759; found, 1148.7786. Anal. Calcd (%) for $C_{42}H_{36}Fe_4O_{10}P_2S_4$: C, 45.27; H, 3.26. Found: C, 45.75; H, 3.72.

Synthesis of [{μ-$(SCH_2)_2N(CH_2CH_2CH_3)$}$Fe_2(CO)_5(Ph_2PCH_2)$]$_2$ (4) and [{μ-$(SCH_2)_2N(CH_2CH_2CH_3)$}$Fe_2(CO)_5${$Ph_2PCH_2CH_2$-(Ph_2PS)}] (5). A solution of **2** (0.215 g, 0.5 mmol) and $Me_3NO\cdot 2H_2O$ (0.111 g, 1 mmol) in CH_3CN (40 mL) was stirred for 5 to 10 min at room temperature. Then, a solution of CH_2Cl_2 (2 mL) with dppe (0.199 g, 0.5 mmol) was added. After 1 h, the solvent was evaporated, and the residue was washed with CH_2Cl_2/hexane (1/1 v/v) to give **4** (181 mg, 60%) and **5** (95 mg, 23%). **4.** ^{1}H NMR ($CDCl_3$): δ 0.66 (s, 6H, 2 × CH_3), 0.88 (s, 4H, 2 × $CH_3CH_2CH_2$), 1.25 (s, 4H, 2 × CH_2CH_2N), 2.08 (s, 4H, PCH_2CH_2P), 2.12 (s, 4H, 2 × NCH_2S), 2.66 (s, 4H, 2 × NCH_2S), 7.37 (s, 12H, Ph), 7.62 (s, 8H, Ph) ppm. ^{13}C NMR ($CDCl_3$): δ 11.71, 29.89, 51.90, 61.81, 88.09, 128.71, 130.10, 132.60, 209.65 ppm. ^{31}P NMR ($CDCl_3$): δ 60.45 (s) ppm. IR (KBr): ν(CO) 2040, 1970 and 1936 cm^{-1}. MS (API−ES): *m*/*z* 1200.8 $[M + H]^+$. Anal. Calcd (%) for $C_{46}H_{46}Fe_4N_2O_{10}P_2S_4$: C, 46.02; H, 3.86; N, 2.33. Found: C, 45.40; H, 4.14; N, 2.33. **5.** ^{1}H NMR ($CDCl_3$): δ 0.66 (s, 3H, CH_3), 0.99 (s, 2H, $CH_3CH_2CH_2$), 1.26 (s, 2H, CH_2CH_2N), 2.57−2.69 (m, 8H, 2 × NCH_2S, PCH_2CH_2P), 7.40 (s, 12H, Ph), 7.69 (d, $J = 40.0$ Hz, 8H, Ph) ppm. ^{13}C NMR ($CDCl_3$): δ 12.90, 29.90, 50.04, 61.18, 128.56, 129.04, 131.29, 132.31, 132.68, 209.66 ppm. ^{31}P NMR ($CDCl_3$): δ 45.33 (d, $J = 132.0$ Hz), 59.56 (d, $J = 132.0$ Hz) ppm. IR (KBr): ν(CO) 2043, 1978, and 1927 cm^{-1}; ν(P═S) 693 cm^{-1}. MS (API−ES): *m*/*z* 831.8 $[M + H]^+$. HRMS (ESI): *m*/*z* calcd for $C_{36}H_{36}Fe_2NO_5S_3P_2$, 831.9929; found, 831.9957. Anal. Calcd (%) for $C_{36}H_{35}Fe_2NO_5P_2S_3$: C, 52.00; H, 4.24; N, 1.68. Found: C, 52.39; H, 4.32; N, 1.70.

Synthesis of [{μ-$(SCH_2)_2CH_2$}$Fe_2(CO)_5(Ph_2PCH_2PPh_2)$] (6). A solution of **1** (0.12 g, 0.31 mmol) and $Me_3NO\cdot 2H_2O$ (0.07 g, 0.63 mmol) in CH_3CN (20 mL) was stirred at room temperature for 15 min. Then, dppm (0.12 g, 0.31 mmol) was added. After stirring for 4 h, the solvent was removed under reduced pressure, and the crude product was purified by chromatography on silica gel with pentane/EtOAc (10:1 v/v) as the eluent. Complex **6** was obtained as a red solid (0.179 g, 77%). ^{1}H NMR ($CDCl_3$): δ 1.61−1.65 (m, 4H, 2 × SCH_2CH_2), 1.71−1.92 (m, 2H, $CH_2CH_2CH_2$), 3.15−3.45 (m, 2H, PCH_2P), 7.10−7.40 (m, 16H, Ph), 7.40−7.80 (m, 4H, Ph) ppm. ^{31}P NMR ($CDCl_3$): δ 58.35 (d, $J = 207.3$ Hz), −25.29 (d, $J = 207.3$ Hz) ppm. IR (KBr): ν(CO) 2040, 1974, 1969, 1960, and 1916 cm^{-1}. Anal. Calcd (%) for $C_{33}H_{28}Fe_2O_3P_2S_2$: C, 53.39; H, 3.80; Found: C, 53.39; H, 3.87.

Synthesis of [{μ-$(SCH_2)_2CH_2$}$Fe_2(CO)_4${μ-$(Ph_2P)_2CH_2$}] (7). A solution of **2** (0.1 g, 0.26 mmol), dppm (0.1 g, 0.26 mmol), and $Me_3NO\cdot 2H_2O$ (0.087 g, 0.78 mmol) in toluene (25 mL) was refluxed for 18 h. The solvent was then removed under reduced pressure, and the crude product was purified by chromatography on silica gel with CH_2Cl_2/pentane (1/3 v/v) as the eluent. Complex **7** was obtained as a red solid (0.6 g, 27%). ^{1}H NMR ($CDCl_3$): δ 1.91−2.01 (m, 2H, $CH_2CH_2CH_2$), 2.09−2.23 (m, 4H, 2 × SCH_2CH_2), 3.10−3.30 (m, 1H, P−CH_2−P), 3.61−3.81 (m, 1H, P−CH_2−P), 7.28−7.50 (m, 16H, Ph), 7.50−7.70 (m, 4H, Ph) ppm. ^{31}P NMR ($CDCl_3$): δ 53.65 (s) ppm. IR (KBr): ν(CO) 1981, 1946, 1916,

(38) Oxford Diffraction. *Xcalibur CCD System, CrysAlis Software System*, Version 1.170; Oxford Diffraction Ltd.: Oxfordshire, U.K., 2003.
(39) *X-RED, Absorption Correction Program*, Version 1.09; Stoe & Cie GmbH: Darmstadt, Germany.
(40) *X-SHAPE, Crystal Optimisation for Numerical Absorption Correction*, version 1.2; Stoe & Cie GmbH: Darmstadt, Germany.
(41) Sheldrick, G. M. *Acta Crystallogr., Sect. A* **1990**, *46*, 467−473.
(42) Sheldrick, G. M. *Computer Program for the Refinement of Crystal Structures*; Göttingen, Germany.

and 1895 cm^{-1}. Anal. Calcd (%) for $C_{32}H_{28}Fe_2O_4P_2S_2 \cdot C_5H_{12} \cdot H_2O$: C, 55.2; H, 5.22. Found: C, 55.4; H, 5.24.

Synthesis of [{μ-(SCH$_2$)$_2$N(CH$_2$CH$_2$CH$_3$)}Fe$_2$(CO)$_5$-(Ph$_2$PCH$_2$PPh$_2$)] (8). A solution of **2** (0.215 g, 0.5 mmol) and dppm (0.192 g, 0.5 mmol) in toluene (40 mL) was refluxed for 0.5 h. Then, the solvent was removed under reduced pressure, and the crude product purified by chromatography on silica gel with CH_2Cl_2/hexane (1/2 v/v) as the eluent. Complex **8** was obtained as a red solid (0.196 g, 50%). ^{1}H NMR ($CDCl_3$): δ 0.70 (t, J = 7.2 Hz, 3H, CH_3), 1.12−1.14 (m, 2H, CH$_3$CH_2CH$_2$), 2.2 (s, 2H, CH$_2$CH_2N), 2.74 (d, J = 9.2 Hz, 2H, NCH_2S), 2.90 (d, J = 9.2 Hz, 2H, NCH_2S), 3.29 (d, J = 9.2 Hz, 2H, PCH_2P), 7.19−7.21 (m, 8H, Ph), 7.26−7.29 (m, 8H, Ph), 7.62 (t, J = 8.8 Hz, 4H, Ph) ppm. ^{31}P NMR ($CDCl_3$): δ 57.76 (d, J = 219 Hz), −25.20 (d, J = 219 Hz) ppm. IR (KBr): ν(CO) 2040, 1977, and 1927 cm^{-1}. Anal. Calcd (%) for $C_{35}H_{33}Fe_2NO_5P_2S_2$: C, 53.52; H, 4.24; N, 1.78. Found: C, 53.56; H, 4.35; N, 1.77.

Synthesis of [{μ-(SCH$_2$)$_2$N(CH$_2$CH$_2$CH$_3$)}Fe$_2$(CO)$_4${μ-(Ph$_2$P)$_2$CH$_2$}] (9). A solution of **2** (0.215 g, 0.5 mmol) and dppm (0.192 g, 0.5 mmol) in toluene (40 mL) was refluxed for 1 h. The solvent was then removed under reduced pressure, and the crude product was purified by chromatography on silica gel with CH_2Cl_2/hexane (1/2 v/v) as the eluent. Complex **7** was obtained as a red solid (0.379 g, 75%). ^{1}H NMR ($CDCl_3$): δ 0.84 (s, 3H, CH_3), 1.26 (s, 2H, CH$_3$CH_2CH$_2$), 1.33 (s, 2H, CH$_2$CH_2N), 3.01 (s, 4H, PCH_2P), 3.81 (s, 2H, NCH_2S), 3.92 (s, 2H, NCH_2S), 7.32 (s, 12H, Ph), 7.59 (s, 8H, Ph) ppm. ^{31}P NMR ($CDCl_3$): δ 54.24 (s) ppm. IR (KBr): ν(CO) 1986, 1952, and 1916 cm^{-1}. Anal. Calcd (%) for $C_{34}H_{33}Fe_2NO_4P_2S_2$: C, 53.92; H, 4.39; N, 1.85. Found: C, 53.40; H, 4.54; N, 1.78.

Protonation of 4. A small amount of **4** (3 mg) was dissolved in CD_3CN (0.5 mL) in an NMR tube, and then, 2.2 μL of triflic acid (5 equiv) was added directly to the solution for in situ ^{1}H NMR, ^{31}P NMR, and IR analysis. **4H$_2$**$^{2+}$. ^{1}H NMR (CD_3CN): δ 0.79 (s, 6H, 2 × CH_3), 0.93 (s, 4H, 2 × CH$_3$CH_2CH$_2$), 1.38 (s, 4H, 2 × CH$_2$CH_2N), 2.77 (m, 4H, PCH_2CH_2P), 3.05 (d, 8H, J = 10.4 Hz, 4 × NCH_2S), 4.30 (m, 8H, 4 × NCH_2S), 7.46 (s, 12H, Ph), 7.62 (s, 4H, Ph), 7.76 (s, 4H, Ph) ppm. ^{31}P NMR (CD_3CN): δ 62.50 (s) ppm. IR (CD_3CN): ν(CO) 2058, 1986, and 1954 cm^{-1}.

The solution of **4H$_2$**$^{2+}$ in CD_3CN was fully deprotonated when aniline (5 equiv) was added. It gave the deposit of **4**, which was identified after filtration by ^{1}H NMR, ^{31}P NMR, and IR in $CDCl_3$. However, when the same amount of 4-cyanoaniline was added, no change happened, thus placing its pK_a between 10.6 and 7.6.

A similar procedure was done to **3** in CD_3CN in an attempt to give **3H$_2$**$^{2+}$. However, we did not obtain a solution just like that of **4H$_2$**$^{2+}$. The ^{1}H NMR, ^{31}P NMR, and IR spectra in ($CDCl_3$) were the same as those of with **3**, just as expected, even when triflic acid was added. This provided evidence that **3** did not react with triflic acid without the participation of the electron during CV.

Control Experiment. In order to confirm the two-electron assignment for the first reduction wave of complexes **3** and **4**, a control experiment was performed. When the total charge (Q) passed during bulk electrolysis at an applied potential of −2.0 V, calculated values for the passage of 1.50, 1.75, and 2.10 electrons were approached.[43] The CVs obtained at the theoretical values of 1.50 and 1.75 electrons per molecule of **3** and **4** also showed a reduction wave at about −1.90 V, although the height of this wave was decreased. However, a CV obtained at the theoretical value of

(43) Tye, J. W.; Lee, J.; Wang, H.-W.; Mejia-Rodriguez, R.; Reibenspies, J. H.; Hall, M. B.; Darensbourg, M. Y. *Inorg. Chem.* **2005**, *44*, 5550−5552.

Table 8. X-ray Crystallographic Data

	3	**4**	**5**	**6**	**7**	**8**	**9**
empirical formula	$C_{42}H_{36}Fe_4O_{10}P_2S_4$	$C_{46}H_{46}Fe_4N_2O_{10}P_2S_4$	$C_{36}H_{35}Fe_2NO_5P_2S_3$	$C_{33}H_{28}Fe_2O_5P_2S_2$	$C_{32}H_{28}Fe_2O_4P_2S_2$	$C_{34}H_{33}Fe_2NO_4P_2S_2$	$C_{34}H_{33}Fe_2NO_4P_2S_2$
fw	1114.29	1200.43	831.47	742.31	714.305	757.37	757.37
crystal system	monoclinic	triclinic	monoclinic	monoclinic	orthorhombic	monoclinic	monoclinic
space group	*C*2/*c*	*P*1	*C*2/*c*	$P2_1/c$	*Pnma*	$P2_1/c$	$P2_1/c$
a (Å)	18.365(5)	10.9853(2)	16.776(7)	9.8480(10)	16.4811(5)	21.5441(10)	21.5441(10)
b (Å)	16.886(4)	11.2692(2)	13.903(6)	14.3088(15)	41.0436(10)	9.7792(4)	9.7792(4)
c (Å)	15.569(4)	12.8333(3)	33.670(13)	23.615(2)	21.3835(7)	16.8278(7)	16.8278(7)
α (°)	90.00	104.3780(10)	90.00	90.00	90.00	90.00	90.00
β (°)	104.217(4)	93.1110 (10)	96.909(6)	90.938	90.00	98.837(3)	98.837(3)
γ (°)	90	118.5390(10)	90.00	90.00	90.00	90.00	90.00
V (Å^3)	4680(2)	1320.49(5)	7796(5)	3327.2(6)	14464.7(7)	3503.3(3)	3503.3(3)
Z	4	1	8	4	16	4	4
ρ_{calcd} (g m^{-3})	1.581	1.510	1.417	1.482	1.312	1.436	1.436
T (K)	293(2)	293(2)	293(2)	295(2)	293(2)	273(2)	273(2)
μ (mm^{-1})	1.516	1.350	1.028	1.133	1.037	1.076	1.076
F (000)	2264	614	3424	1520	5856	1560	1560
reflns collected	9614	6825	17065	19010	134322	24548	24548
reflns/R_{int}	4109/0.0622	4572/0.0186	8408/0.0421	10680/0.07671	24626/0.4113	7404/ 0.0316	7404/ 0.0316
GOF (on F^2)	1.171	1.074	1.015	0.820	0.792	0.999	0.999
R1 [$I > 2\sigma(I)$] (all data)[a]	0.0796 (0.1207)	0.0490 (0.0541)	0.0593 (0.1194)	0.0480 (0.2303)	0.0821(0.4680)	0.0657(0.0437)	0.0657(0.0437)
wR2 [$I > 2\sigma(I)$] (all data)[b]	0.1328 (0.1456)	0.1413 (0.1480)	0.1244 (0.1470)	0.0874 (0.1269)	0.1714(0.3037)	0.1429(0.1285)	0.1429(0.1285)

[a] $R1 = (\sum||F_o| - |F_c||)/(\sum|F_o|)$. [b] $wR2 = [\sum w(F_o^2 - F_c^2)^2/\sum w(F_o^2)^2]^{1/2}$.

ca. 2.10 and 2.13 electrons per molecule for **3** and **4** did not show any reduction wave at −1.90 V, indicating the complete reduction of the bulk solution.

Acknowledgment. We are grateful to the Ministry of Science and Technology of China (Grant No. 2001CCA02500), the Chinese National Natural Science Foundation (Grant No. 20633020), the Swedish Energy Agency, and the Swedish Research Council for financial support. We also thank to Ms. Rong Zhang for the HRMS measurements and Ms. Kun Jin for the NMR measurements.

Supporting Information Available: Crystallographic information files (CIF) for **3**−**9** and cyclic voltammograms for **3**, **4**, **7**, and **9**. This material is available free of charge via the Internet at http://pubs.acs.org.

IC0610278